RSC Advances

PAPER

View Article Online
View Journal | View Issue

Cite this: *RSC Adv.*, 2018, **8**, 37105

Catalytic effect of $(H_2O)_n$ (n = 1–3) on the $HO_2 + NH_2 \rightarrow NH_3 + {}^3O_2$ reaction under tropospheric conditions†

Tianlei Zhang,* Kai Wang,‡ Zhangyu Qiao,‡ Yongqi Zhang,‡ Lin Geng,‡ Rui Wang, Zhiyin Wang, Caibin Zhao and Linxia Jin*

The effects of $(H_2O)_n$ (n = 1–3) clusters on the $HO_2 + NH_2 \rightarrow NH_3 + {}^3O_2$ reaction have been investigated by employing high-level quantum chemical calculations with M06-2X and CCSD(T) theoretical methods, and canonical variational transition (CVT) state theory with small curvature tunneling (SCT) correction. The calculated results show that two kinds of reaction, $HO_2\cdots(H_2O)_n$ (n = 1–3) + NH_2 and $H_2N\cdots(H_2O)_n$ (n = 1–3) + HO_2, are involved in the $(H_2O)_n$ (n = 1–3) catalyzed $HO_2 + NH_2 \rightarrow NH_3 + {}^3O_2$ reaction. Due to the fact that $HO_2\cdots(H_2O)_n$ (n = 1–3) complexes have much larger stabilization energies and much higher concentrations than the corresponding complexes of $H_2N\cdots(H_2O)_n$ (n = 1–3), the atmospheric relevance of the former reaction is more obvious with its effective rate constant of about 1–11 orders of magnitude faster than the corresponding latter reaction at 298 K. Meanwhile, due to the effective rate constant of the $H_2O\cdots HO_2 + NH_2$ reaction being respectively larger by 5–6 and 6–7 orders of magnitude than the corresponding reactions of $HO_2\cdots(H_2O)_2 + NH_2$ and $HO_2\cdots(H_2O)_3 + NH_2$, the catalytic effect of $(H_2O)_n$ (n = 1–3) is mainly taken from the contribution of the water monomer. In addition, the enhancement factor $(k_t'(WM1a)/k_{tot})$ of the water monomer is 10.06–13.30% within the temperature range of 275–320 K, which shows that at whole calculated temperatures, a positive water effect is obvious under atmospheric conditions.

Received 3rd August 2018
Accepted 23rd October 2018

DOI: 10.1039/c8ra06549g

rsc.li/rsc-advances

1. Introduction

The hydroperoxyl radical (HO_2) and amidogen radical (NH_2) are two important reactive radicals in atmospheric processes and combustion chemistry. As one of the most abundant free radicals in the atmosphere, HO_2 is a very important and reactive intermediate in atmospheric pollutant degradation,[1,2] photocatalysis,[3] and molecular oxygen activation on metal surfaces[4,5] or in enzymes.[6] Produced from the gas phase oxidation of ammonia (NH_3) by the hydroxyl radical (eqn (1)), NH_2 is not only interesting in the combustion of fossil fuels, but is also considered to play an important role in the atmospheric formation and elimination of NO_x (ref. 7) and in the oxygen isotopic exchange of N_2O. Meanwhile, NH_2 reacts with nitric acid can regenerate ammonia (eqn (2)). This reaction and the reaction shown in eqn (1) have been proposed as a potential new catalytic-like cycle which couples the oxidation of ammonia by hydroxyl radicals and the reaction of nitric acid with amidogen radicals in the Earth's atmosphere.[8] Based on these facts, the kinetics and mechanism of the $NH_2 + HO_2$ reaction (eqn (3)) have been studied experimentally and theoretically.[9–15]

$$NH_3 + HO \rightarrow NH_2 + H_2O \quad (1)$$

$$NH_2 + HNO_3 \rightarrow NH_3 + NO_3 \quad (2)$$

$$NH_2 + HO_2 \rightarrow NH_3 + O_2 \quad (3)$$

On experimental aspect, Sarkisov *et al.*[10] have measured the gas-phase reaction between NH_2 and HO_2 by the analytical technique of the VIS-UV absorption at a total pressure of 133–9.33×10^4 Pa and the rate constant of the reaction (3) has been found to be 7.51×10^{-11} cm^3 per molecule per s at 300 K. Meanwhile, the rate constant of $NH_2 + HO_2$ reaction has been estimated indirectly by flash-photolysis, which is 2.5×10^{-11} cm^3 per molecule per s at 300 K.[9] Theoretically, Sumathi *et al.*[14] obtained the singlet potential energy surface of reaction (3) at QCISD(T)/6–311++ G(2*df*,2*pd*)//6–311++G**/MP2 level. In their work, to obtain the ratio of their product formation and to estimate the contribution of different channels over a wide range of temperature, the primary concern is to analyze the

Institute of Theoretical and Computational Chemistry, Shaanxi Key Laboratory of Catalysis, School of Chemical & Environment Science, Shaanxi University of Technology, Hanzhong, Shaanxi 723001, China. E-mail: ztianlei88@163.com; jinlx@snut.edu.cn; Fax: +86-0916-2641083; Tel: +86-0916-2641083

† Electronic supplementary information (ESI) available. See DOI: 10.1039/c8ra06549g

‡ Kai Wang, Zhangyu Qiao, Yongqi Zhang and Lin Geng contributed equally to this work.

competition among the various reaction channels. However, the triplet potential energy surface of reaction (3), especially, the triplet hydrogen abstraction (HA) is not involved, which is not neglected for the HA in many previous reports reaction between radical and HO_2 radical.[16–30] Even in some HA reaction, triplet HA is favorable kinetically.[16,18,20,23,26,29,30] So, both the singlet and triplet HA have been investigated at the CCSD(T)//B3LYP/6–311++G(3*df*,3*pd*) level by Xiang *et al.*[31] In their work, for the favorable HA, the reaction mechanism on the triplet potential surface to be mainly a barrierless addition of HO_2 to NH_2 leading to an intermediate $OOH\cdots NH_2$ (^{3}im1), and then the adduct ^{3}im1 goes through an H transfer forming the product of NH_3 and $^3O_2$.

These investigations provide meaningful information about the HA of $NH_2 + HO_2$ reaction under atmospheric conditions. Nevertheless, these studies did not take into consideration the influence of water vapors on the reaction. In fact, firstly, water is ubiquitous in the Earth's atmosphere and its monomer can form hydrogen bonded complexes with other abundant radicals changing their photochemical features.[32] Such as previous investigations showed that in the process of HO_2 self-reaction, hydrogen bonded complexes $HO_2\cdots H_2O$ are formed with approximately 30% of the HO_2 in the atmosphere bonding with water under typical atmospheric conditions.[33] Another example is that water monomer can bind with NH_2 radical, forming $H_2O\cdots H_2N$, and $H_2N\cdots H_2O$ complexes.[34] Secondly, it is also known that water was found to actively participate in the atmospheric reactions of $HO_2 + HO_2$,[25,35] $HO_2 + HS$,[28] $HO_2 + HO$,[26,36] $HO_2 + SO_2$,[37] $HO_2 + NO_2$ (ref. 24) and $HO_2 + O_3$ (ref. 38 and 39) reactions. Meanwhile, in these processes, water vapor had a catalytic effect by increasing the stability of pre-reactive complexes and reducing the activation energy of transition states. The above facts forecast that it cannot ignore water in modeling the different atmospheric HA reactions. These situations stimulated our interest in modeling the gas-phase reaction of $H_2O\cdots HO_2\cdots NH_2$ ternary system, in which the single water molecule serves as a catalyst.

Although atmospheric water molecule implies a significant catalytic effect by monomers, the catalytic effect of water dimers and also water trimers can't be ignored, because their concentrations are up to 9×10^{14} and 2.6×10^{12} molecules per cm^3 at 298 K.[40,41] Moreover, the experimental and theoretical studies have been reported in the literature on the electronic structure of the clusters $HO_2\cdots(H_2O)_n$ (n = 2–3).[28,39] Thus, the catalytic effects of $(H_2O)_n$ (n = 2–3) are worth being investigated further on the $HO_2 + NH_2 \rightarrow NH_3 + {}^3O_2$ reaction.

In the present study, based on the $HO_2 + NH_2 \rightarrow NH_3 + {}^3O_2$ reaction without water molecule, a detailed effects of $(H_2O)_n$ (n = 1–3) on the HA reaction of $HO_2 + NH_2 \rightarrow NH_3 + {}^3O_2$ have been studied at the CCSD(T)/CBS//M06-2X/6-311+G(3*df*,2*pd*) level of theory, which is organized as follows: firstly, the triplet HA reaction of $HO_2 + NH_2 \rightarrow NH_3 + {}^3O_2$ was investigated to compare with $(H_2O)_n$ (n = 1–3)-assisted processes. Secondly, the reactions of $H_2O\cdots HO_2 + NH_2$, $HO_2\cdots H_2O + NH_2$, $H_2O\cdots H_2N + HO_2$ and $H_2N\cdots H_2O + HO_2$ with water monomer were evaluated by investigating direct HA process and double hydrogen transfer mechanism. In what follows, direct HA processes of $HO_2\cdots(H_2O)_2$ (water dimer and the whole HO_2 radical formed a ring by hydrogen bonds) + NH_2, $HO_2\cdots(H_2O)_2$–I (water dimer and the HO moiety of HO_2 radical formed a ring by hydrogen bonds) + NH_2 and $H_2N\cdots(H_2O)_2 + HO_2$ reactions with $(H_2O)_2$ were also calculated. Then, based on the discussed results of water dimer, the reactions of $HO_2\cdots(H_2O)_3 + NH_2$ and $H_2N\cdots(H_2O)_3 + HO_2$ were mainly investigated for the channel of $NH_3 + {}^3O_2$ formations with water trimer. Finally, the effective rate constants of the HA reaction of $HO_2 + NH_2 \rightarrow NH_3 + {}^3O_2$ with $(H_2O)_n$ (n = 1–3) were calculated to investigate the atmospheric relevance of the effect of $(H_2O)_n$ (n = 1–3). Overall, this work may lead to a better understanding of the effects of $(H_2O)_n$ (n = 1–3) on the gas-phase reactions under tropospheric conditions.

2. Computational methods

2.1 Electronic structure calculation

The electronic structure calculations were performed using Gaussian 09 program package[42] software. The geometries of all the reactants, intermediates, transition states and products have been optimized using the M06-2X[43–46] method using the 6-311+G(3*df*,2*pd*) basis set. The corresponding frequencies of the optimized geometries were computed at the same level to confirm the characteristics of the transition states with one imaginary frequency and the stationary points without imaginary frequency. Moreover, the minimum energy path (MEP) was obtained by the intrinsic reaction coordinate (IRC)[47–49] theory with a gradient step size of 0.01 − 0.05 $(amu)^{1/2}$ bohr to prove that the TS connects to minima along the reaction path. In order to obtain more accurate relative energies, single-point energy calculations for the stationary points were performed at the CCSD(T) method[50] in conjunction with CBS basis set based on the M06-2X/6-311+G(3*df*,2*pd*)-optimized geometries. The single point energy calculations of CCSD(T)/CBS have been carried out for all the species at CCSD(T) level of theory using aug-*cc*-pVDZ and aug-*cc*-pVTZ basis sets. The energy values obtained at DZ and TZ levels have been used to extrapolate the results to a complete basis set (CBS) limit.[51]

2.2 Rate constant calculations

To estimate the effect of $(H_2O)_n$ (n = 1–3) added, the theoretical rate constants of canonical variational transition (CVT) state theory[52–54] with small curvature tunneling (SCT) correction[55,56] for every H-abstraction channels were calculated by employing VKLab program[57] coupled with the steady state approximation.

In the presence of $(H_2O)_n$ (n = 1–3), all the processes for the formations of NH_3 and $^3O_2$ from the reaction of HO_2 and NH_2 involve two major steps as follows.

$$\text{Step a:}\quad A + B \underset{k_{-1}}{\overset{k_1}{\rightleftharpoons}} C$$

$$\text{Step b:}\quad C + D \underset{k_{-2}}{\overset{k_2}{\rightleftharpoons}} E \xrightarrow{k_{uni}} F$$

Here, A and B are any two among HO_2, NH_2 and $(H_2O)_n$ (n = 1–3) clusters (water monomer, WM; water dimer, WD; and water trimer, WT), C is the binary complex formed by A and B. D is the remaining third species other than A and B. E is the ternary complex formed by HO_2, NH_2 and $(H_2O)_n$ (n = 1–3). In the step a, A combines with B to from an adduct C, whereas the step b consists of two elementary processes: in the first one, C reacts with D to form E and subsequently E undergoes uni-molecular transformation to produce the formation F *via* the corresponding TS.

Assuming that the intermediate E was in equilibrium with the corresponding reactants (C and D) and was at steady state,[58] the rate constant for step b can be written as

$$k_b = \frac{k_2}{k_{-2} + k_{uni}} k_{uni} \quad (4)$$

If $k_{uni} \ll k_{-2}$, the rate constant of k_b was rewritten as

$$k_b = \frac{k_2}{k_{-2} + k_{uni}} k_{uni} = K_{eq_2} k_{uni} \quad (5)$$

The rate constant k_{uni} in eqn (5) has been evaluated by VKLab program[57] in the framework of the canonical variational transition state theory (CVT).[54] To include the tunneling effects for motion along the reaction coordinate for the title reactions at the CCSD(T)/CBS//M06-2X/6-311+G(3*df*,2*pd*) level, the small curvature tunneling (SCT)[55] approximation has been adopted in this study. Besides, K_{eq_2} in eqn (5) was given by eqn (6).

$$K_{eq_2}(T) = \sigma \frac{Q_E}{Q_C Q_D} \exp\left(\frac{E_D + E_C - E_E}{RT}\right) \quad (6)$$

In eqn (6), the various Q values denote the partition functions of the intermediate E, reactants C and D, respectively. All partition functions were obtained using the M06-2X/6-311+G(3*df*,2*pd*) method. E_D, E_C and E_E stand for the energies of the species of D, C and E, respectively; σ is the symmetry factor. In the present work, k_b has been used to compare the rates between bare reaction and catalyzed reactions.

2.3 Effective rate constant calculations

If one incorporates the effect of step a, the resultant rate constant (k_t) can be written as:

$$k_t = K_{eq_1} K_{eq_2} k_{uni} \quad (7)$$

where K_{eq_1} stands for the equilibrium constant in step a *i.e.* $K_{eq_1} = k_1/k_{-1}$, and K_{eq_1} was given by eqn (8).

$$K_{eq_1}(T) = \sigma \frac{Q_C}{Q_A Q_B} \exp\left(\frac{E_A + E_B - E_C}{RT}\right) \quad (8)$$

In eqn (8), the various Q values denote the partition functions of the complex C, reactants A and B, respectively. E_A, E_B and E_C stand for the energies of the species of A, B and C, respectively. From the above, the rate of the reaction (v) in the presence of catalysts can be written as:

$$v = K_{eq_1} K_{eq_2} k_{uni}[A][B][D] = k_t[A][B][D] = k'_t[A][B] \quad (9)$$

k'_t is the effective rate constant, which could be considered as a measure of the relative efficiencies of the different catalysts under atmospheric conditions, as it includes the concentration as well as rate constant of a particular catalyst.

3. Results and discussion

The transition states in each reaction channel were signed by "TS" followed by a number, and intermediates were denoted by "IM" followed by a number. The letters "a", "b", and "c" were used to distinguish the transition states and intermediates that were conformers of each other and therefore had the same features; a species in the presence of water monomer, water dimer and water trimer was respectively denoted by a "WM", "WD", and "WT" suffix.

3.1 Potential energy surfaces and the rate constants for the hydrogen abstraction of $HO_2 + NH_2 \rightarrow NH_3 + {}^3O_2$ reaction

The $HO_2 + NH_2 \rightarrow NH_3 + {}^3O_2$ reaction was investigated theoretically by Xiang *et al.*[31] at the CCSD(T)/6–311++G(3*df*,3*pd*)//B3LYP/6–311++G(3*df*,3*pd*) level. In this study, we have reinvestigated that work at the CCSD(T)/CBS//M06-2X/6-311+G(3*df*,2*pd*) level to determine the outcome of this reaction when $(H_2O)_n$ (n = 1–3) was present. As seen in Fig. 1, regarding the HA reaction of $HO_2 + NH_2$ to produce $NH_3 + {}^3O_2$, only one elementary reaction path was identified (Channel R1). Starting from $HO_2 + NH_2$ reactants, Channel R1 began with the intermediate IM. The binding energy of IM was 6.9 kcal mol^{-1}, agree with that (^{3}im1, 7.4 kcal mol^{-1}) in the literature reported by Xiang *et al.*[31] For IM, from geometrical point of view, a hydrogen bond shown in Fig. 1 was formed between the H atom of HO_2 and the N atom of NH_2 radical (with a computed H···N bond distance of 1.81 Å at the M06-2X/6-311+G(3*df*,2*pd*) level of theory). With the N atom of NH_2 radical attacks the H atom of HO_2, the intermediate IM in Channel R1 proceeded through a transition state TS with the energy predicted to be at 4.5 kcal mol^{-1} below the initial reactants. The energy of TS is quite different from ^{3}ts3 (6.8 kcal mol^{-1} below $HO_2 + NH_2$

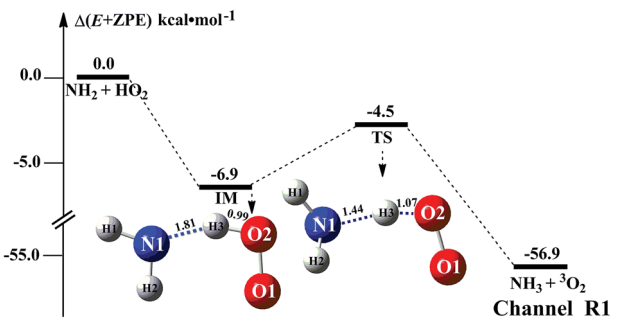

Fig. 1 Schematic energy diagram for the $HO_2 + NH_2$ reaction; energies (kcal mol^{-1}) at the CCSD(T)/CBS//M06-2X/6-311+G(3*df*,2*pd*)) level of theory.

reactants) in the literature reported by Xiang *et al.*[31] This difference is possible due to the fact that the different levels of theory used for the ZPE and single-point energy calculation. Besides, the ΔH (298) of $HO_2 + NH_2 \rightarrow NH_3 + {}^3O_2$ reaction was predicted to be -57.0 kcal mol^{-1}, compared with the experimental[59] estimation of -58.5 ± 0.4 kcal mol^{-1}. For reaction (1) without water, Table S1† lists its CVT/SCT rate constant. As seen in Table S1,† tunneling slightly increases the rate constant, while the recrossing effects decrease the rate constant. For example, the rate constant is increased by 62% due to tunneling, while the rate constant is decreased to 52% because of recrossing effects at the M06-2X/6-311+G(3*df*,2*pd*) level and at 298 K (Table S1†). It is noted that tunneling and recrossing effects slightly depend on temperature. Tunneling slightly increases with the decrease of temperature, while recrossing effects slightly increase with the increase of temperature as listed in Table S1.† Specifically, the calculated results using M06-2X/aug-*cc*-pVTZ indicate that the rate constant is increased by 32% and 20% due to tunneling, while the rate constant is decreased to 44% and 60% at 275 and 320 K, respectively. So, similar with previous investigations,[60,61] the tunneling transmission coefficients are very large for the hydrogen atom transfer process. Thus, herein the computed CVT/SCT rate constants have been used to estimate the catalytic effect of $(H_2O)_n$ (n = 1–3). CVT/SCT rate constant calculations were carried out for Channel R1 at various temperatures. The values are listed in Table S1.† At 300 K, the calculated value of k_{R_1} was 2.68×10^{-11} cm^3 per molecule per s. The calculated values compare closely with 7.51×10^{-11} cm^3 per molecule per s and 2.5×10^{-11} cm^3 per molecule per s, at 300 K respectively predicted by Sarkisov *et al.*[10] and Cheskis *et al.*[9] indicating that the calculations for the $HO_2 + NH_2 \rightarrow NH_3 + {}^3O_2$ reaction without and with $(H_2O)_n$ (n = 1–3) at the CCSD(T)/CBS//M06-2X/6-311+G(3*df*,2*pd*) level of theory are acceptable.

3.2 Geometrical analysis and the concentration calculation for $HO_2\cdots(H_2O)_n$ (n = 1–3) and $H_2N\cdots(H_2O)_n$ (n = 1–3) complexes

In the presence of $(H_2O)_n$ (n = 1–3), both bodies of HO_2 and NH_2 can respectively interact with the second body of $(H_2O)_n$ (n = 1–3) *via* hydrogen bond to form two-body complexes of $HO_2\cdots(H_2O)_n$ (n = 1–3) and $H_2N\cdots(H_2O)_n$ (n = 1–3) first in the entrance channels before interacting with the third body of NH_2 or HO_2. So, it is very necessary to find the stable configurations of the complexes $HO_2\cdots(H_2O)_n$ (n = 1–3) and $H_2N\cdots(H_2O)_n$ (n = 1–3) firstly. In order to find all possible stable configurations of the complexes $HO_2\cdots(H_2O)_n$ (n = 1–3) and $H_2N\cdots(H_2O)_n$ (n = 1–3), the global minimum searching of geometric structures were carried out using Tsinghua Global Minimum (TGMin).[62,63] Then the initial structures for $HO_2\cdots(H_2O)_n$ (n = 1–3) and $H_2N\cdots(H_2O)_n$ (n = 1–3) were selected for geometry optimization using the M06-2X/6-31G(*d*) method. The isomer structures within 6.0 kcal mol^{-1} of the global minimum were re-optimized by M06-2X/6-311+G(3*df*,2*pd*) method. The Fig. 2 and S1† show the optimized geometrical reactants of $HO_2\cdots(H_2O)_n$ (n = 1–3) and $H_2N\cdots(H_2O)_n$ (n = 1–3), which are in good agreement with available previous results.[64,65] As seen in Fig. 2 and S1,† as the number of water molecules increases in a given cluster of $HO_2\cdots(H_2O)_n$ (n = 1–3) and $H_2N\cdots(H_2O)_n$ (n = 1–3), the number of possible configurations for the cluster increases quickly, and each of the configurations becomes increasingly complicated. Regarding to each type equilibrium structure of $HO_2\cdots(H_2O)_n$ (n = 1–3) and $H_2N\cdots(H_2O)_n$ (n = 1–3), herein we only focus on the stable configuration shown in Fig. 2, which has the larger stabilization energy and the higher concentration than its isomers.

As seen in Fig. 2 and Table S2,† consistent with previous reports,[24,25,28,37,66] five-membered ring complex $H_2O\cdots HO_2$ was much more stable than the single hydrogen bond complexes $HO_2\cdots H_2O$, $H_2N\cdots H_2O$ and $H_2O\cdots H_2N$ with its binding energy larger by 3.6–5.9 kcal mol^{-1} than those of latter ones. The equilibrium constants of these complexes at 298 K are 1.83×10^{-19}, 3.05×10^{-22}, 1.34×10^{-22} and 8.40×10^{-21} cm^3 per molecule, respectively (Table S3†). Considering typical tropospheric concentrations of 7.73×10^{17} molecules per cm^3 of H_2O, 3×10^8 molecules per cm^3 of HO_2,[67] and our estimated concentrations of NH_2 (6.0×10^{-11} molecules per cm^3 seen in ESI†), it is estimated that the atmospheric concentration of the $H_2O\cdots HO_2$ complex to be 4.24×10^7 molecules per cm^3, which is larger by 6.00×10^2 times than that of $HO_2\cdots H_2O$. However, in our previous works,[25,26] the reaction channels of $HO_2\cdots H_2O + HO_2$ and $HO_2\cdots H_2O + HO$ were not neglected in water-catalyzed $HO_2 + HO_2$ and $HO_2 + HO$. So, for water catalyzed $HO_2 + NH_2 \rightarrow NH_3 + {}^3O_2$ reaction, both $H_2O\cdots HO_2 + NH_2$ and $HO_2\cdots H_2O + NH_2$ reactions have been investigated in the following section. Besides these, at 298 K, the concentrations of $H_2N\cdots H_2O$ (3.90×10^{-13} cm^3 per molecule) and $H_2O\cdots H_2N$ (6.21×10^{-15} cm^3 per molecule) shown in Table S3† were much lower than those of $H_2O\cdots HO_2$ (4.24×10^7 cm^3 per molecule) and $HO_2\cdots H_2O$ (7.07×10^4 cm^3 per molecule). Thus, in water catalyzed $HO_2 + NH_2 \rightarrow NH_3 + {}^3O_2$ reaction, we predict that the atmospheric relevance of $H_2O\cdots HO_2 + NH_2$ and $HO_2\cdots H_2O + NH_2$ reactions will be much more obvious than those of $H_2N\cdots H_2O + HO_2$ and $H_2O\cdots H_2N + HO_2$ reactions. Thus, only $H_2O\cdots HO_2 + NH_2$ and $HO_2\cdots H_2O + NH_2$ reactions have been taken into account in the following section, whereas, for comparison, the potential energy surfaces (PESs) for $H_2N\cdots H_2O + HO_2$ and $H_2O\cdots H_2N + HO_2$ reactions has been displayed in Fig. S5,† and their corresponding rate constants were shown in Table S7.†

For the clusters constituted by HO_2 (or NH_2) radical and water dimer, in geometrical point of view, $HO_2\cdots(H_2O)_2$ (water dimer and the whole HO_2 radical formed a ring by hydrogen bonds) shows seven-membered ring structure, whereas both $HO_2\cdots(H_2O)_2$–I (water dimer and the HO moiety of HO_2 radical formed a ring by hydrogen bonds) and $H_2N\cdots(H_2O)_2$ involves a six-membered ring. So, the binding energy of $HO_2\cdots(H_2O)_2$ (shown in Table S2†) was 12.6 kcal mol^{-1}, which was larger by 3.9–6.4 kcal mol^{-1} than those of $HO_2\cdots(H_2O)_2$–I and $H_2N\cdots(H_2O)_2$ due to smaller ring tension. Similarity, nine-membered ring $HO_2\cdots(H_2O)_3$ (water trimer and the whole HO_2 radical formed a ring by hydrogen bonds) was larger by 2.0–7.3 kcal mol^{-1} than those of eight-membered ring $HO_2\cdots(H_2O)_3$–I (water trimer and the HO moiety of HO_2 radical formed a ring by hydrogen bonds)

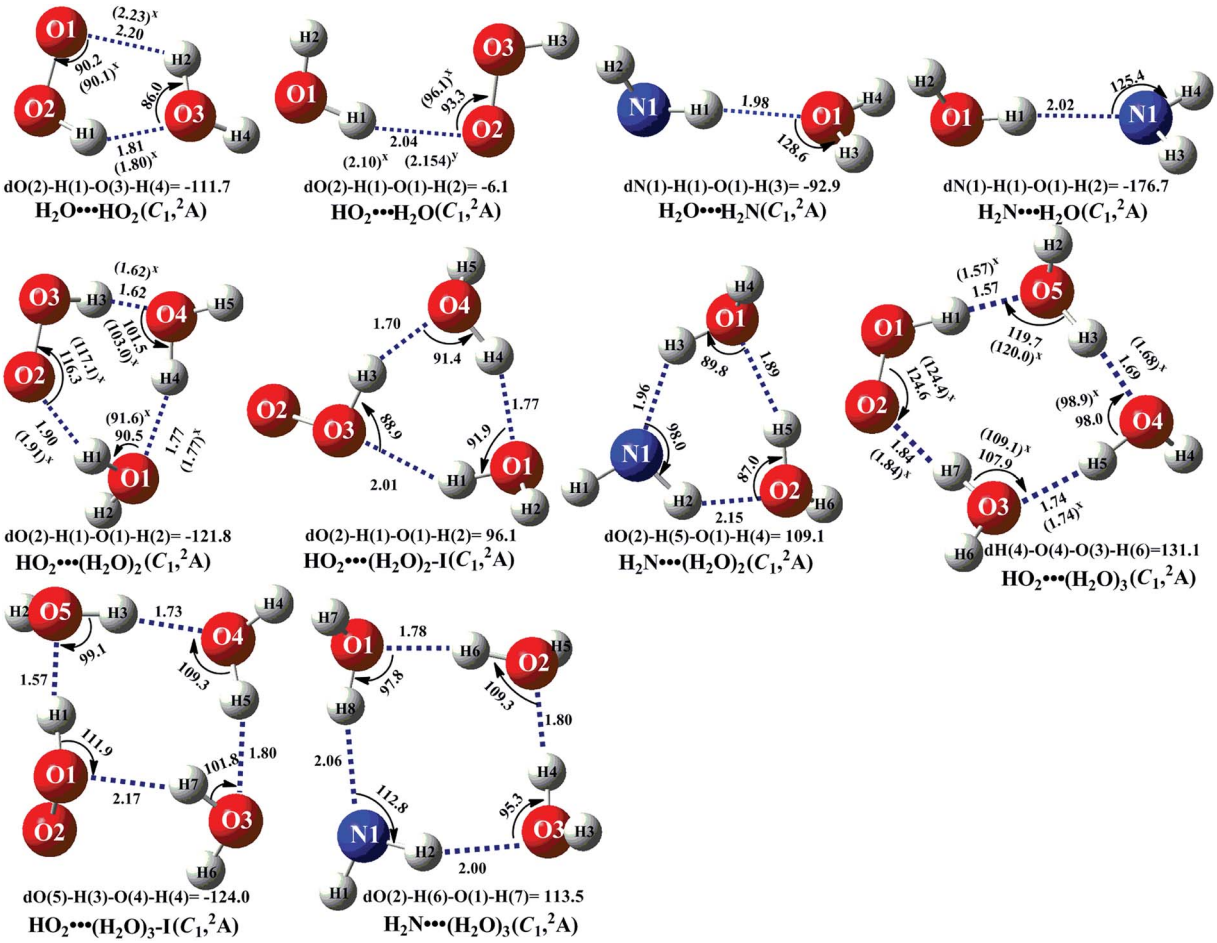

Fig. 2 The geometrical structures of the optimized complexes at the M06-2X/6-311+G(3*df*,2*pd*) level of theory (bond length Å, bond angle °).

and $H_2N\cdots(H_2O)_3$. From another point of view shown in Table S3,† the concentrations of $H_2N\cdots(H_2O)_2$ (5.13×10^{-17} cm^3 per molecule) and $H_2N\cdots(H_2O)_3$ (1.02×10^{-19} cm^3 per molecule) are also much lower than those of $HO_2\cdots(H_2O)_2$ (5.14×10^{5} cm^3 per molecule) and $HO_2\cdots(H_2O)_3$ (8.02×10^{3} cm^3 per molecule) at 298 K, thus we predict that the atmospheric relevance of $H_2N\cdots(H_2O)_2 + HO_2$ and $H_2N\cdots(H_2O)_3 + HO_2$ reactions can be neglected. However, for comparison, the PESs for $H_2N\cdots(H_2O)_2 + HO_2$ and $H_2N\cdots(H_2O)_3 + HO_2$ reactions have been displayed in Fig. S6 and S7,† and their corresponding rate constants were shown in Table S7.† Besides these, the concentrations of $HO_2\cdots(H_2O)_2$ and $HO_2\cdots(H_2O)_3$ are respectively larger by 140 and 9 times than the corresponding complexes of $HO_2\cdots(H_2O)_2$–I and $HO_2\cdots(H_2O)_3$–I at 298 K. So, we predict that the catalytic effect of $HO_2\cdots(H_2O)_2$–I + NH_2 and $HO_2\cdots(H_2O)_3$–I + NH_2 reactions are less obvious than the corresponding reactions of $HO_2\cdots(H_2O)_2 + NH_2$ and $HO_2\cdots(H_2O)_3 + NH_2$.

3.3 Potential energy surfaces and the rate constants for $HO_2 + NH_2 \rightarrow NH_3 + {}^3O_2$ reaction with H_2O

It has been pointed out in Section 3.2 that water-catalyzed the reaction (3) is mainly occurring through $H_2O\cdots HO_2 + NH_2$ and $HO_2\cdots H_2O + NH_2$ reactions. So, Fig. 3 presents the PESs for $H_2O\cdots HO_2 + NH_2$ (Channel WM1) and $HO_2\cdots H_2O + NH_2$ (Channel WM2) reactions along with the local minimum geometries on the corresponding reaction pathways.

Regarding to Channel WM1, by different collisions between $H_2O\cdots HO_2$ and NH_2, two kinds of reaction types have been found, which were labeled as Channel WM1a and Channel WM1b. For Channel WM1a, starting from $H_2O\cdots HO_2 + NH_2$ reactants, hydrogen-bonded complex IM_WM1 was formed by the interaction between N atom of NH_2 radical and one H atom of the H_2O moiety in $H_2O\cdots HO_2$ complex with a bonding energy of 5.5 kcal mol^{-1}. After a flat potential energy surface through TS_WM1, with an energy barrier of 4.3 kcal mol^{-1}, the formation of seven-member cyclic complex IM_WM2 was formed with a binding energy of 7.3 kcal mol^{-1} relative to $H_2O\cdots HO_2 + NH_2$ reactants. Following complex IM_WM2, Channel WM1a proceeded through transition state TS_WM2 to produce the product of $NH_3\cdots H_2O$ and $^3O_2$ after climbing the barrier height of 3.4 kcal mol^{-1}. In the transition state TS_WM2, the seven-membered ring structure was still conserved with the N atom of NH_2 radical abstracting the H atom of HO_2 moiety in $H_2O\cdots HO_2$ complex.

Similar with Channel WM1a, Channel WM1b also followed stepwise process. In the first step, similar with the ring enlargement from IM_WM1 to IM_WM2 in Channel WM1a, the

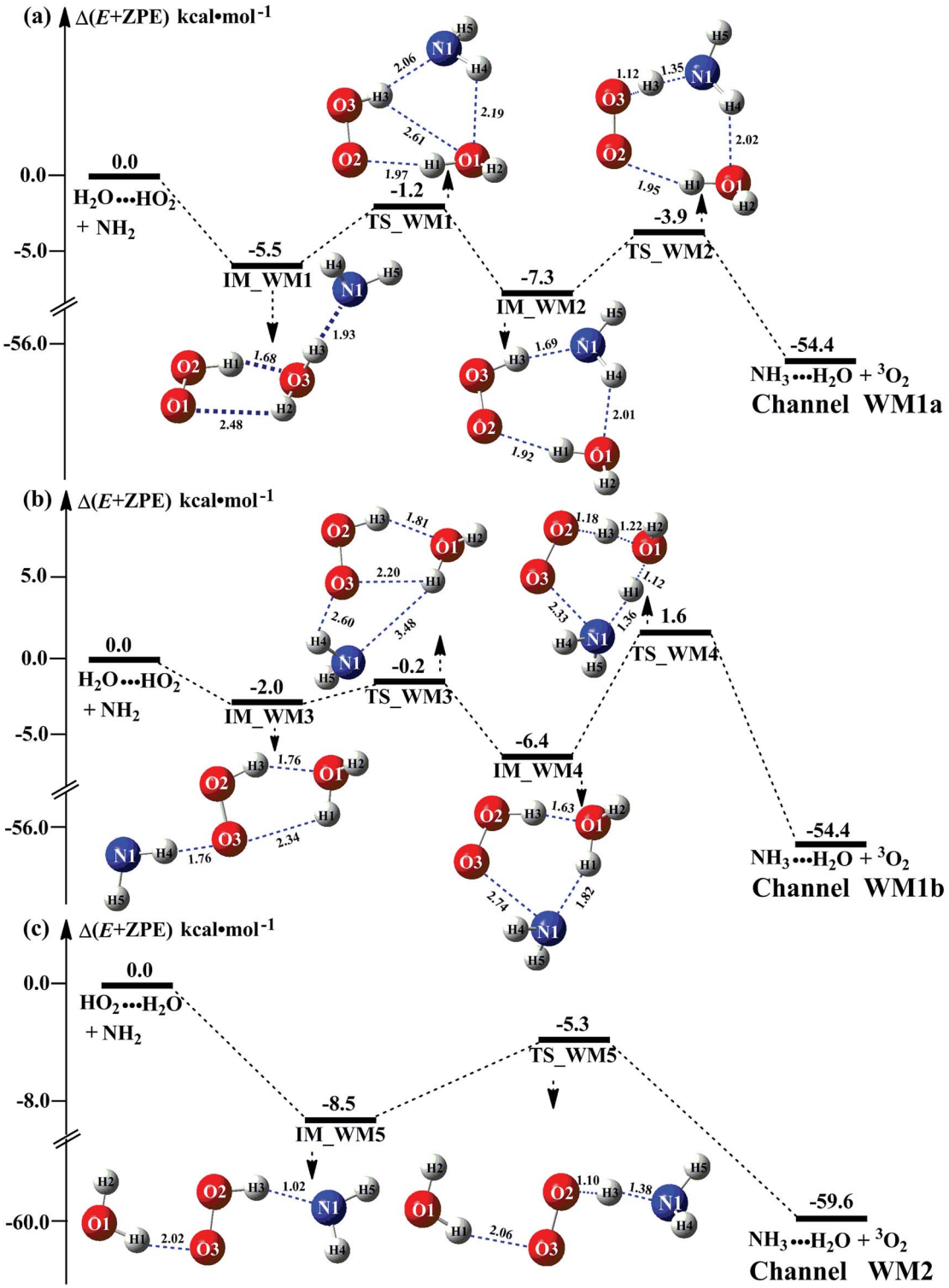

Fig. 3 Schematic energy diagram for the water assisted $HO_2 + NH_2 \rightarrow NH_3 + {}^3O_2$ reaction occurring through $H_2O\cdots HO_2 + NH_2$ (a and b), and $HO_2\cdots H_2O + NH_2$ (c) reactions; energies (kcal mol^{-1}) at the CCSD(T)/CBS//M06-2X/6-311+G(3*df*,2*pd*) level of theory.

five-membered ring complex IM_WM3 is rearranged into seven-membered ring complex IM_WM4 through TS_WM3. In geometrical point of view, complex IM_WM4 has similar seven-membered cyclic structure as IM_WM2 with the NH_2 radical and the water molecule exchanging their positions. The binding energy of IM_WM4 is 6.4 kcal mol^{-1}, lowered by 0.9 kcal mol^{-1} than that of IM_WM2. In the second step, differently from transition state TS_WM2 in Channel WM1a that involves a direct HA, transition state TS_WM4 in Channel WM1b contains a double hydrogen transfer mechanism. Consistent

Table 1 Rate constants (cm^3 per molecule per s) of the $HO_2 + NH_2 \rightarrow NH_3 + {}^3O_2$ reaction with $(H_2O)_n (n = 1–3)^{a,b}$

T(K)	k_b(WM1a)	k_b(WM1b)	k_b(WM2)	k_b(WD1)	k_b(WD2)	k_b(WT1)
275	6.53×10^{-11}	6.36×10^{-15}	2.21×10^{-11}	1.35×10^{-15}	1.84×10^{-17}	1.47×10^{-14}
280	5.23×10^{-11}	5.85×10^{-15}	1.70×10^{-11}	1.39×10^{-15}	1.92×10^{-17}	1.45×10^{-14}
290	3.46×10^{-11}	5.00×10^{-15}	1.04×10^{-11}	1.48×10^{-15}	2.07×10^{-17}	1.42×10^{-14}
298	2.54×10^{-11}	4.44×10^{-15}	7.19×10^{-12}	1.56×10^{-15}	2.20×10^{-17}	1.41×10^{-14}
300	2.38×10^{-11}	4.32×10^{-15}	6.62×10^{-12}	1.58×10^{-15}	2.23×10^{-17}	1.40×10^{-14}
310	1.68×10^{-11}	3.79×10^{-15}	4.34×10^{-12}	1.68×10^{-15}	2.39×10^{-17}	1.39×10^{-14}
320	1.23×10^{-11}	3.35×10^{-15}	2.92×10^{-12}	1.78×10^{-15}	2.55×10^{-17}	1.38×10^{-14}

[a] k_b(WM1a), k_b(WM1b), k_b(WM2) and k_b(WD1), k_b(WD2), k_b(WT1) is the rate constants of $(H_2O)_n$ ($n = 1–3$)-assisted $HO_2 + NH_2 \rightarrow NH_3 + {}^3O_2$ reaction occurring through Channels WM1a, WM1b, WM2 WD1, WD2, and WT1, respectively. [b] $1/k_{uni}$(WM1a) = $1/k$(TS_WM1) + $1/k$(TS_WM2); $1/k_{uni}$(WM1b) = $1/k$(TS_WM3) + $1/k$(TS_WM4); $1/k_{uni}$(WD1) = $1/k$(TS_WD1) + $1/k$(TS_WD2); $1/k_{uni}$(WT1) = $1/k$(TS_WT1) + $1/k$(TS_WT2).

with our previous reports,[28] such mechanism discrepancy between Channels WM1a and WM1b may lead that the energy barrier of the second step in Channel WM1a is 3.4 kcal mol^{-1}, which is lower by 4.6 kcal mol^{-1} than that of the second step in Channel WM1b. The reason can be possibly explained in three following aspects: (1) transition state TS_WM2 in the former reaction shows seven-member ring structure, whereas the transition state TS_WM4 in the latter reaction shows six-member ring structure. That is, TS_WM4 has larger ring tension than that of TS_WM2; (2) different from the structures in the process of IM_WM4 → TS_WM4 where the three hydrogen atoms (H2, H4 and H5) are out of plane, the structure in the process of IM_WM2 → TS_WM2 is close to the coplanar structure, which makes the conjugated hydrogen bonding system (H3⋯N1, H4⋯O1 and H1⋯O2) more stable; (3) NBO charge analysis shows that (Fig. S8†), the distance between the negatively NBO charged O3 and N1 atoms was decreases from IM-WM4 (2.70 Å) → TS-WM4 (2.33 Å), resulting in enhanced repulsive interactions, and hence the energy of the system is increased.

As shown in Table 1, it is worth noting that the rate constants both of Channel WM1a (k_b(WM1a)) and Channel WM1b (k_b(WM1b)) are increased with the decrease of temperature. This is because the calculated bimolecular rate constant contains two different components, (see Table S7†)); (1) K_{eq} from the first step (bimolecular addition between $H_2O\cdots HO_2$ and NH_2) and (2) k_2 from the second step (IM_WM1 (or IM_WM3) → $NH_3\cdots H_2O + {}^3O_2$). The second step always contributes to the positive activation energy due to the finite positive barrier, while the first step corresponds to negative activation energy as it involves barrierless addition of isolated reactants to form the complex IM_WM1 (or IM_WM3). Consequently, K_{eq} always decreases with increase in temperature, whereas k_2 behaves in opposite manner (Table S7†). Whenever k_2 dominates over K_{eq} the overall activation energy of the reaction is found to be positive and when K_{eq} dominates over k_2 then the overall activation energy of the reaction become negative. For example, for Channel RW1a, K_{eq} decreases by ~6.69 times and k_2 value increases ~1.26 times with increasing temperature from 275 to 320 K. The rate constant of Channel WM1a (k_b(WM1a)) within the temperature range of 275–320 K is much larger than the corresponding value of k_b(WM1b) in Channel WM1b, given that the ratio of k_b(WM1a)/k_b(WM1b) is 3.67×10^3 to 1.03×10^4. As a result, in the following section, the reaction type where water dimer and water trimer act as a "bridge" will not be considered in the reactions between $HO_2\cdots(H_2O)_2 + NH_2$ and $HO_2\cdots(H_2O)_3 + NH_2$.

Differently from Channel WM1a and Channel WM1b above which involve a stepwise process, $HO_2\cdots H_2O + NH_2$ reaction (Channel WM2) contains a one-step mechanism. As for Channel WM2, the reaction started with the formation of a pre-reactive hydrogen bond complex IM_WM5. Compared with the naked complex IM (Fig. 1), in view of geometry, complex IM_WM5 was stabilized by an additional weak hydrogen bond (O3⋯H1, 2.02 Å) and thus, the binding energy of IM_WM5 was enhanced by 1.6 kcal mol^{-1} than that of IM. Starting from IM_WM5, Channel WM2 proceeded through transition state TS_WM5, which is similar in structure to the naked transition state TS, where the N atom of NH_2 radical directly abstracted the hydrogen of HO_2. The rate constant of Channel WM2 (k_b(WM2)) listed in Table 1 is only lower by 3–4 times than the corresponding value of k_b(WM1a) in Channel WM1a. However, for $H_2O\cdots HO_2$ complex, both the concentration and equilibrium constant at 298 K is larger by 2 orders of magnitude than that of $HO_2\cdots H_2O$. As a result, atmospheric relevance of $H_2O\cdots HO_2 + NH_2$ reaction occurring through directing HA will be obvious than that of $HO_2\cdots H_2O + NH_2$ reaction. Besides these, compared with the rate constant of $H_2N\cdots H_2O + HO_2$ reaction (k_b(WM3)) listed in Table S7,† though the value of k_b(WM1a) is smaller by 2 orders of magnitude, atmospheric relevance of $H_2N\cdots H_2O + HO_2$ reaction will be neglected with respect to $H_2O\cdots HO_2 + NH_2$ reaction, due to the fact that the concentration of $H_2N\cdots H_2O$ complex is much lower than that of $H_2O\cdots HO_2$. This result can be further proved by the effective rate constant in the following section. So, atmospheric relevance of $H_2O\cdots HO_2 + NH_2$ reaction occurring through directing HA will be most obvious in water monomer catalyzed $HO_2 + NH_2 \rightarrow NH_3 + {}^3O_2$ reaction.

3.4 Potential energy surfaces and the rate constants for $HO_2 + NH_2 \rightarrow NH_3 + {}^3O_2$ reaction with $(H_2O)_2$

As the discussion in Section 3.2 that the atmospheric relevance of $HO_2\cdots(H_2O)_2 + NH_2$ reaction is most obvious in water dimer-catalyzed the reaction (3). So, Fig. 4 shows the PESs of $HO_2\cdots(H_2O)_2 + NH_2$ reaction (Channel WD1) with its rate constant

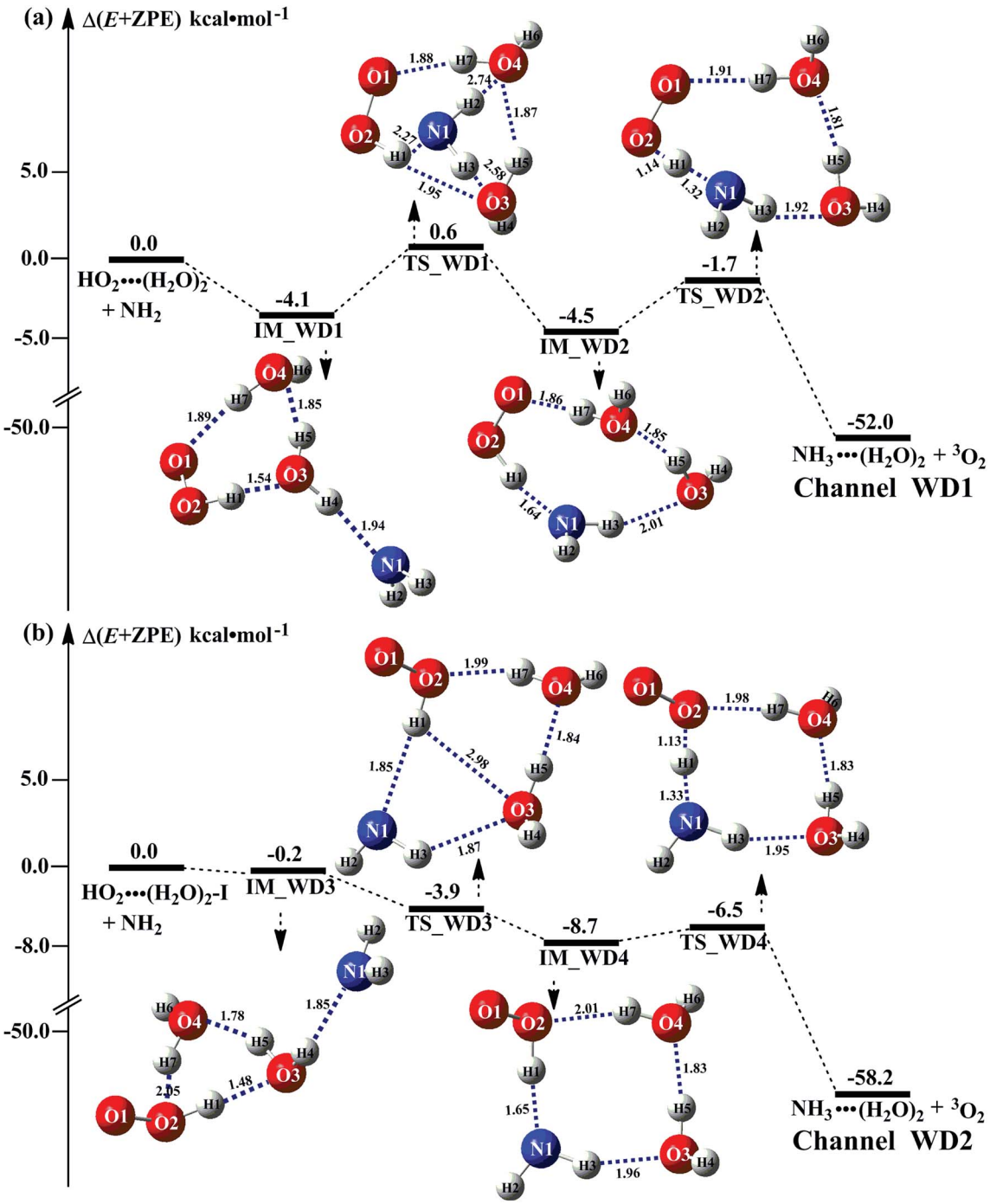

Fig. 4 Schematic energy diagrams for water dimer-assisted $HO_2 + NH_2 \rightarrow NH_3 + {}^3O_2$ reaction occurring through $HO_2\cdots(H_2O)_2 + NH_2$ (a) and $HO_2\cdots(H_2O)_2$–I + NH_2 (b) reactions; energies (kcal mol^{-1}) at the CCSD(T)/CBS//M06-2X/6-311+G(3*df*,2*pd*) level of theory.

listed in Table 1. For comparison, PESs for $HO_2\cdots(H_2O)_2$–I + NH_2 reaction (Channel WD2) was displayed in Fig. 4, and its corresponding rate constant was shown in Table 1.

For Channels WD1 and WD2 shown in Fig. 4, both reactions proceeded through a stepwise mechanism, where the reaction firstly occurred *via* a ring enlargement, and then proceed through a direct HA. However, the rate constant of Channel WD2 (k_b(WD2)) listed in Table 1 is much smaller than the corresponding value of k_b(WD1) in Channel WD1, given that the ratio of k_b(WD1)/k_b(WD2) is 69.8–73.4. Meanwhile, the value of k_b(WD1) is larger by 6 orders of magnitude than that of k_b(WD3) ($H_2N\cdots(H_2O)_2 + HO_2$ reaction). Thus, for the reaction (3) with water dimer, $HO_2\cdots(H_2O)_2 + NH_2$ reaction (Channel WD1) is of great atmospheric relevance due to its larger rate constant, and only this channel has been mainly taken into account here.

Consistent with the favorable channel of $H_2O\cdots HO_2$ + NH_2 reaction (Channel WM1a) above, as for Channel WD1, with the collision between NH_2 and $HO_2\cdots(H_2O)_2$, the reaction occurred *via* a stepwise mechanism. In the first step, Channel WD1 went through a ring enlargement from seven-membered ring complex IM_WD1 to nine-membered ring complex IM_WD2 *via* transition state TS_WD1 with an energy barrier of 4.7 kcal mol^{-1}. In geometrical point of view, complexes IM_WD1 and IM_WD2 have similar structures as the corresponding complexes of IM_WM1 and IM_WM2, expecting that water monomer was substituted by water dimer. So, in energetic point of view, similar with the fact that the complex IM_WM2 in Channel WM1a (Fig. 3) is more stable than IM_WM1, complex IM_WD2 in Channel WD1 is stable than IM_WD1. However, the stabilization energy of IM_WD2 has been reduced by 2.8 kcal mol^{-1} than that of IM_WM2. In the second step, following IM_WD2 complex, with the N atom of NH_2 abstracting the H atom of HO_2 moiety in $HO_2\cdots(H_2O)_2$, Channel WD1 can proceed *via* an elementary reaction of direct HA (TS_WD2) to form the products of $NH_3\cdots(H_2O)_2$ + $^3O_2$. Similar with complex IM_WD2, TS_WD2 also shows a nine-membered ring structure with water dimer, NH_2 radical and HO_2 radical involved. The relative energy of TS_WD2 to $HO_2\cdots(H_2O)_2$ + NH_2 is −1.7 kcal mol^{-1}, which is higher by 2.2 kcal mol^{-1} than that of the water-assisted transition state TS_WM2 to $H_2O\cdots HO_2$ + NH_2 reactants. Meanwhile, the rate constant of Channel WD1, as shown in Table 1, is smaller by 3–4 orders of magnitude than that of k_b(WM1a) with single water. Due to the fact that $H_2O\cdots HO_2$ has higher concentration than that of $HO_2\cdots(H_2O)_2$, we predict that Channel WD1 has less obvious positive influence on enhancing the rate of the reaction (eqn (3)) than Channels WM1a.

3.5 Potential energy surfaces and the rate constants for HO_2 + NH_2 → NH_3 + $^3O_2$ reaction with $(H_2O)_3$

It is of interest to known whether $(H_2O)_3$ will affect the HO_2 + NH_2 → NH_3 + $^3O_2$ reaction. Thus, based on the discussed results above that the reaction of NH_2 radical with $HO_2\cdots(H_2O)_2$ is more favorable than the reactions of NH_2 radical with $HO_2\cdots(H_2O)_2$–I in the presence of water dimer, only the reaction of NH_2 radical with $HO_2\cdots(H_2O)_3$ was mainly investigated for the channel of NH_3 + $^3O_2$ formations with water trimer due to that the binding energy (Table S2†) and the concentration (Table S3†) of $HO_2\cdots(H_2O)_3$ are much larger than those of $H_2N\cdots(H_2O)_3$, $HO_2\cdots(H_2O)_3$–I. The schematic potential energy surfaces for $HO_2\cdots(H_2O)_3$ + NH_2 reaction was shown in Fig. 5, meanwhile its rate constant is also listed in Table 1, which is larger by 6 orders of magnitude than that of k_b(WT2) ($H_2N\cdots(H_2O)_3$ + HO_2 reaction) involved in Table S7.†

Regarding the reaction of $HO_2\cdots(H_2O)_3$ + NH_2, the pre-reactive complex IM_WT1 was formed with the energy of 1.1 kcal mol^{-1} with respect to the $HO_2\cdots(H_2O)_3$ + NH_2 reactants. Starting from complex IM_WT1, the reaction occurs *via*

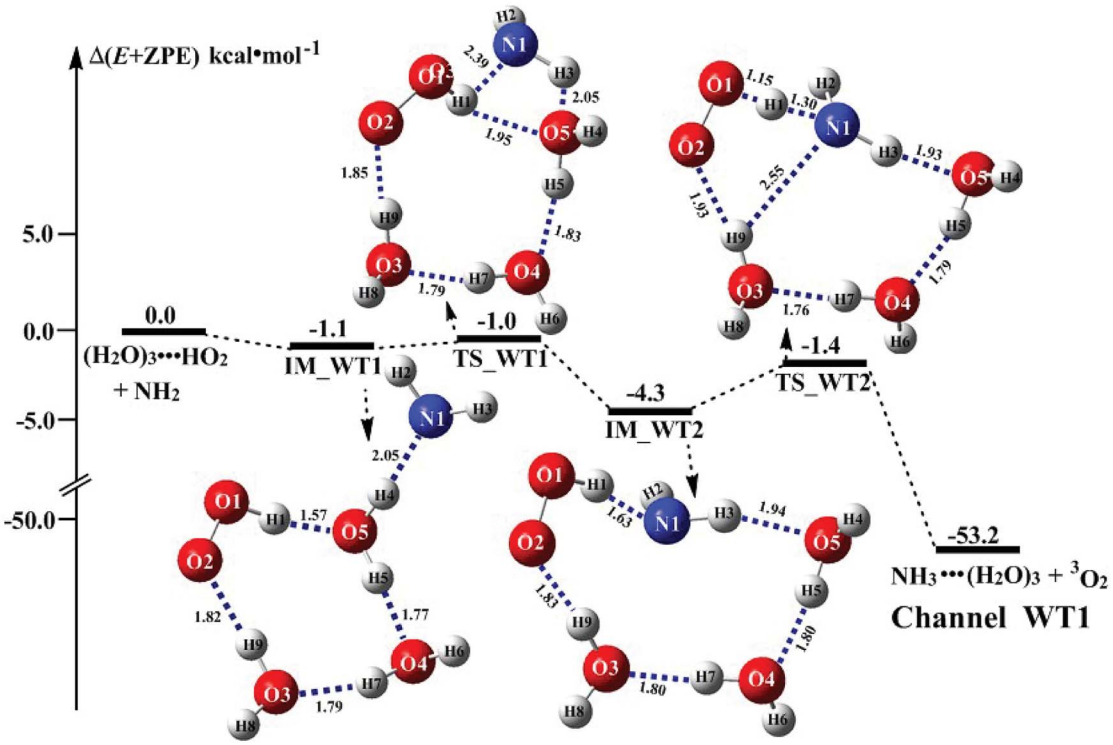

Fig. 5 Schematic energy diagrams for water trimer-assisted HO_2 + NH_2 → NH_3 + $^3O_2$ reaction occurring through $HO_2\cdots(H_2O)_3$ + NH_2(a) reactions; energies (kcal mol^{-1}) at the CCSD(T)/CBS//M06-2X/6-311+G(3*df*,2*pd*) level of theory. [x]Value was from ref. and key interatomic distances (angstroms) and angles (degrees) of molecular structures was given at the M06-2X/aug-*cc*-pVTZ. [y]Value was from ref. and key interatomic distances (angstroms) and angles (degrees) of molecular structures was given at the MP2/6-31G* level of theory.

transition state TS_WT1 and to form a complex IM_WT2 with a barrier of 0.1 kcal mol^{-1} relative to the pre-reactive complex IM_WT1. This step involves a geometric rearrangement that plays a crucial role in $HO_2\cdots(H_2O)_3 + NH_2$ reaction. IM_WT2 is more stabilized than IM_WT1 by 3.2 kcal mol^{-1}. From the geometric point of view, complex IM_WT2 has similar quasi-planar structure as that of IM_WD2 with the additional water molecule inserted between HO_2 and NH_2. The relative energy of IM_WT2 is −4.3 kcal mol^{-1} with respect to $HO_2\cdots(H_2O)_3 + NH_2$.

Transition state TS_WT2 was found between IM_WT2 and the products ($H_3N\cdots(H_2O)_3$ and $^3O_2$). For the TS_WT2, a HA reaction occurs by the N atom of NH_2 abstracted the H atom of HO_2 radical as that in TS_WD2 with the additional water molecule inserted between HO_2 and NH_2. TS_WT2 lies 1.4 kcal mol^{-1} below the $HO_2\cdots(H_2O)_3 + NH_2$ reactants, which is 0.3 kcal mol^{-1} higher in energy than the relative energy of TS_WD2 to $HO_2\cdots(H_2O)_2 + NH_2$ reactants. Meanwhile, the rate constant of Channel WT1 (shown in Table 1) is larger by 8–11 times than that of k_b(WD1) with water dimer. Due to the fact that $HO_2\cdots(H_2O)_2$ has higher concentration than that of $HO_2\cdots(H_2O)_3$, thus, whether the atmospheric relevance of $HO_2\cdots(H_2O)_3 + NH_2$ reaction is obvious than that of $HO_2\cdots(H_2O)_3 + NH_2$ reaction or not, needs further discussion in the next section.

3.6 Application in atmospheric chemistry

Beyond above mechanisms and rate constant without and with $(H_2O)_n$ (n = 1–3), another aim of our work was to study the influence of $(H_2O)_n$ (n = 1–3) on the $HO_2 + NH_2$ reaction under atmospheric conditions. Thus, it is necessary to compare the title rate in the absence of $(H_2O)_n$ (n = 1–3) with the effective rates of the favorable reactions in the presence of $(H_2O)_n$ (n = 1–3). Table 2 lists the calculated effective rate constants for the favorable channels of $HO_2 + NH_2 \rightarrow NH_3 + {}^3O_2$ reaction without and with $(H_2O)_n$ (n = 1–3). For comparisons, the effective rate constants of other channels have been displayed in Table S7.†

As shown in Table 2, within the temperature range of 275–320 K, the effective rate constant of $H_2O\cdots HO_2 + NH_2$ reaction (k'_t(WM1a)) is 2.42×10^{-12} to 6.02×10^{-12} cm^3 per molecule per s, which is larger by 3 orders of magnitude than the corresponding value of $HO_2\cdots H_2O + NH_2$ reaction (k'_t(WM2)), as shown in Table S7.† Meanwhile, the value of k'_t(WM1a) is respectively larger by 23.5–46.0 and 1.17×10^{10} to 4.10×10^{11} times than the value of k'_t(WM3) ($H_2O\cdots H_2N + HO_2$ reaction) and k'_t(WM4) ($H_2N\cdots H_2O + HO_2$ reaction) listed in Table S7.† This indicates that the catalytic effect of water monomer is mainly taken from $H_2O\cdots HO_2 + NH_2$ reaction.

For the catalytic effect of water dimer, the effective rate constant of $HO_2\cdots(H_2O)_2 + NH_2$($k'_t$(WD1)) is 1.33×10^{-18} to 4.43×10^{-18} cm^3 per molecule per s, which is larger by 3–4 and 9–10 orders of magnitude than the corresponding value of $HO_2\cdots(H_2O)_2$–I + NH_2 reaction k'_t(WD2) and $NH_2\cdots(H_2O)_2 + HO_2$($k'_t$(WD3)) listed in Table S7,† showing that the catalytic effect of water dimer is mainly taken from $HO_2\cdots(H_2O)_2 + NH_2$ reaction. Similarity, the catalytic effect of water trimer is mainly taken from $HO_2\cdots(H_2O)_3 + NH_2$ reaction (k'_t(WT1)), with the rate constant of k'_t(WT1) is larger by 10–11 orders of magnitude than the corresponding value of $NH_2\cdots(H_2O)_3 + HO_2$($k'_t$(WT2)) listed in Table S7.† Besides, the effective rate constant of $HO_2\cdots(H_2O)_2 + NH_2$($k'_t$(WD1)) is larger by 6–10 times than the corresponding value of $HO_2\cdots(H_2O)_3 + NH_2$($k'_t$(WT1)). This shows that compared with water trimer, the catalytic effect of water dimer is not neglected. However, the value of k'_t(WD1) is smaller by 5–6 orders of magnitude than the effective rate constant of $H_2O\cdots HO_2 + NH_2$ reaction (k'_t(WM1a)). So, the catalytic effect of single water is the largest among the effect of water, water dimer and water trimer, and the catalytic effect taken from water dimer and water trimer is neglected.

To obtain a more complete understanding of the influence of a water vapor on the title reaction, it is also necessary to compare the title rate constant (k_{R_1}) in the absence of a water vapor with the effective rate constant of the most favorable channel of $H_2O\cdots HO_2 + NH_2$ reaction (k'_t(WM1a)). The result in Table 2 is also estimated that within the temperature range of 275–320 K, the enhancement factor of water vapor (k'_t(WM1a)/k_{tot}) is 10.06–13.30%, showing, in the whole calculated range, the positive water effect is obvious under atmospheric conditions.

Table 2 Effective rate constants (cm^3 per molecule per s) for the favorable channels of $HO_2 + NH_2 \rightarrow NH_3 + {}^3O_2$ reaction with $(H_2O)_n$ (n = 1–3)[a,b,c]

T(K)	k_{R_1}	k'_t(WM1a)	k'_t(WD1)	k'_t(WT1)	k'_t(WM1a)/k_{tot}
275	5.50×10^{-11}	6.02×10^{-12}	1.33×10^{-18}	1.40×10^{-19}	10.06%
280	4.72×10^{-11}	5.25×10^{-12}	1.51×10^{-18}	1.69×10^{-19}	10.24%
290	3.52×10^{-11}	4.20×10^{-12}	2.05×10^{-18}	2.60×10^{-19}	10.94%
298	2.82×10^{-11}	3.59×10^{-12}	2.64×10^{-18}	3.76×10^{-19}	11.64%
300	2.68×10^{-11}	3.36×10^{-12}	2.77×10^{-18}	4.05×10^{-19}	11.47%
310	2.08×10^{-11}	2.90×10^{-12}	3.59×10^{-18}	5.90×10^{-19}	12.64%
320	1.64×10^{-11}	2.42×10^{-12}	4.43×10^{-18}	7.99×10^{-19}	13.30%

[a] Effective rate constants (cm^3 per molecule per s) of k'_t(WM1a) and k'_t(WD1), and k'_t(WT1) have been calculated using 100% relative humidity. [b] $k_{tot} = k_{R_1} + k'_t$(WM), k'_t(WM1a), k'_t(WD1) and k'_t(WT1) is respectively the effective rate constants of $H_2O\cdots HO_2 + NH_2$(a), $HO_2\cdots(H_2O)_2 + NH_2$ and $HO_2\cdots(H_2O)_3 + NH_2$ reaction. [c] k'_t(WM1a) = k_b(WM1a)K_{eq}($H_2O\cdots HO_2$)[H_2O]; k'_t(WD1) = k_b(WD1)K_{eq}($HO_2\cdots(H_2O)_2$)[$(H_2O)_2$]; and k'_t(WT1) = k_b(WT1)K_{eq}($HO_2\cdots(H_2O)_3$)[$(H_2O)_3$]. K_{eq}($H_2O\cdots HO_2$), K_{eq}($HO_2\cdots(H_2O)_2$) and K_{eq}($HO_2\cdots(H_2O)_3$) is respectively the equilibrium constants for the formation of the $H_2O\cdots HO_2$, $HO_2\cdots(H_2O)_2$ and $HO_2\cdots(H_2O)_3$ complexes, whereas [H_2O], [$(H_2O)_2$], and [$(H_2O)_3$] are the concentrations of water vapor, water dimer and water trimer.[65]

4. Summary and conclusions

The $HO_2 + NH_2 \rightarrow NH_3 + {}^3O_2$ reaction catalyzed by $(H_2O)_n$ (n = 1–3) has been studied theoretically using quantum chemical methods and the canonical variational transition state theory, which results in the following conclusions:

(a) Regarding to each type equilibrium structure of $HO_2\cdots(H_2O)_n$ (n = 1–3) and $H_2N\cdots(H_2O)_n$ (n = 1–3), complexes of $H_2O\cdots HO_2$, $HO_2\cdots H_2O$, $HO_2\cdots(H_2O)_2$, and $HO_2\cdots(H_2O)_3$ are the most stable configurations, which have larger stabilization energies and higher concentrations than their isomers, and thus $(H_2O)_n$ (n = 1–3) catalyzed $HO_2 + NH_2 \rightarrow NH_3 + {}^3O_2$ reactions are mainly occurring through four kinds of reactions of $H_2O\cdots HO_2 + NH_2$, $HO_2\cdots H_2O + NH_2$, $HO_2\cdots(H_2O)_2 + NH_2$ and $HO_2\cdots(H_2O)_3 + NH_2$.

(b) For water-assisted $HO_2 + NH_2 \rightarrow NH_3 + {}^3O_2$ reaction, the channel occurring through the $H_2O\cdots HO_2 + NH_2$ reactants may be of great atmospheric relevance due to its larger effective rate constant and the larger concentration of $H_2O\cdots HO_2$. Besides, though $HO_2\cdots H_2O + NH_2$ reaction has lower activation energy, its effective rate constant is smaller by 3 orders of magnitude than the corresponding value of $H_2O\cdots HO_2 + NH_2$ reaction. So, the catalytic effect of water monomer is mainly taken from $H_2O\cdots HO_2 + NH_2$ reaction.

(c) For $HO_2\cdots(H_2O)_2 + NH_2$ and $HO_2\cdots(H_2O)_3 + NH_2$ reactions, both the reactions followed through a stepwise mechanism, where the reaction firstly occurred *via* a ring enlargement, and then proceed through a direct HA. However, the effective rate constant of $H_2O\cdots(H_2O)_2 + NH_2(k'_t(WD1))$ is larger by 6–10 times than the corresponding value of $H_2O\cdots(H_2O)_3 + NH_2(k'_t(WT1))$, showing that compared with water trimer, the catalytic effect of water dimer is not neglected. However, the effective rate constant of $HO_2\cdots(H_2O)_2 + NH_2$ is smaller by 5–6 orders of magnitude than that of $H_2O\cdots HO_2 + NH_2$ reaction, showing that the catalytic effect of single water is the largest among the effect of water, water dimer and water trimer, and the catalytic effect taken from water dimer and water trimer is neglected.

(d) The enhancement factor of water vapor $(k'_t(WM1a)/k_{tot})$ is 10.06–13.30% within the temperature range of 275–320 K, showing that, in the whole calculated range, the positive water effect is obvious under atmospheric conditions.

Conflicts of interest

The authors declare no conflicts of interest.

Acknowledgements

This work was supported by the National Natural Science Foundation of China (No: (21603132), the Funds of Research Programs of Shaanxi University of Technology (No: SLGQD13(2)-3, SLGQD13(2)-4).

References

1 M. Kumar and J. S. Francisco, *Angew. Chem., Int. Ed.*, 2015, **54**, 15711–15714.
2 J. M. Anglada, M. Martins-costa, J. S. Francisco and M. F. Ruiz-lópez, *Acc. Chem. Res.*, 2015, **48**, 575–583.
3 J. C. Colmenares and R. Luque, *Chem. Soc. Rev.*, 2014, **43**, 765–778.
4 Y. Zheng, Y. Jiao, M. Jaroniec and S. Z. Qiao, *Angew. Chem., Int. Ed.*, 2015, **54**, 52–65.
5 C. R. Chang, X. F. Yang, B. Long and J. A. Li, *ACS Catal.*, 2013, **3**, 1693–1699.
6 P. Campomanes, U. Rothlisberger, M. Alfonsoprieto and C. Rovira, *J. Am. Chem. Soc.*, 2015, **137**, 11170–11178.
7 B. J. Finlayson-Pitts and J. N. Pitts Jr, *Chemistry of the Upper and Lower Atmosphere: Theory, Experiments, and Applications*, Academic Press, 1999, pp. 633–637.
8 J. M. Anglada, S. Olivella and A. Solé, *J. Am. Chem. Soc.*, 2014, **136**, 6834–6837.
9 S. G. Cheskis and O. M. Sarkisov, *Chem. Phys. Lett.*, 1979, **62**, 72–76.
10 O. M. Sarkisov, S. G. Cheskis, V. A. Nadtochenko, E. A. Sviridenkov and V. I. Vedeneev, *Arch. Combust.*, 1984, **4**, 111–120.
11 J. W. Bozzelli and A. M. Dean, *J. Phys. Chem.*, 1989, **93**, 1058–1065.
12 D. L. Baulch, C. J. Cobos, R. A. Cox, C. Esser, P. Frank, Th. Just, J. A. Kerr, M. J. Pilling, J. Troe, R. W. Walker and J. Warnatz, *J. Phys. Chem. Ref. Data*, 1992, **21**, 411–734.
13 R. Atkinson, D. L. Baulch, R. A. Cox, R. F. Hampson Jr, J. A. Kerr and J. Troe, *J. Phys. Chem. Ref. Data*, 1989, **18**, 881–1097.
14 R. Sumathi and S. D. Peyerimhoff, *Chem. Phys. Lett.*, 1996, **263**, 742–748.
15 W. B. Demore, S. P. Sander, D. M. Golden, R. F. Hampson, M. J. Kurylo, C. J. Howard, A. R. Ravishankara, C. E. Kolb and M. J. Molina, *JPL Publ.*, 1985, **90**, 1135–1151.
16 J. M. Anglada, S. Olivella and A. Solé, *J. Phys. Chem. A*, 2006, **110**, 6073–6082.
17 E. Assaf, C. Schoemaecker, L. Vereecken and C. Fittschen, *Phys. Chem. Chem. Phys.*, 2018, **20**, 10660–10670.
18 R. Chow, D. K. W. Mok, E. P. F. Lee and J. M. Dyke, *Phys. Chem. Chem. Phys.*, 2016, **18**, 30554–30569.
19 E. Drougas, *Comput. Theor. Chem.*, 2016, **1093**, 98–103.
20 J. M. Anglada, S. Olivella and A. Solé, *J. Phys. Chem. A*, 2007, **111**, 1695–1704.
21 J. Li, N. T. Tsona and L. Du, *Phys. Chem. Chem. Phys.*, 2018, **20**, 10650–10659.
22 L. Vereecken and J. S. Francisco, *Chem. Soc. Rev.*, 2012, **41**, 6259–6293.
23 T. Zhang, G. Li, W. Wang, Y. Du, C. Li and J. Lü, *Comput. Theor. Chem.*, 2012, **991**, 13–21.
24 T. Zhang, R. Wang, H. Chen, S. Min, Z. Wang, C. Zhao, Q. Xu, L. Jin, W. Wang and Z. Wang, *Phys. Chem. Chem. Phys.*, 2015, **17**, 15046–15055.

25 T. Zhang, R. Wang, W. Wang, S. Min, Q. Xu, Z. Wang, C. Zhao and Z. Wang, *Comput. Theor. Chem.*, 2014, **1045**, 135–144.
26 T. Zhang, W. Wang, C. Li, Y. Du and J. Lü, *RSC Adv.*, 2013, **3**, 7381–7391.
27 T. Zhang, W. Wang, P. Zhang, J. Lü and Y. Zhang, *Phys. Chem. Chem. Phys.*, 2011, **13**, 20794–20805.
28 T. Zhang, C. Yang, X. Feng, J. Kang, L. Song, Y. Lu, Z. Wang, Q. Xu, W. Wang and Z. Wang, *Phys. Chem. Chem. Phys.*, 2016, **18**, 17414–17427.
29 Y. Zhang, T. Zhang and W. Wang, *Int. J. Quantum Chem.*, 2011, **111**, 3029–3039.
30 Y. Zhang, W. Zhang, T. Zhang, W. Tian and W. Wang, *Comput. Theor. Chem.*, 2012, **994**, 65–72.
31 T. Xiang, H. Si, P. Han and R. Yang, *Comput. Theor. Chem.*, 2012, **985**, 67–71.
32 R. J. Buszek, J. S. Francisco and J. M. Anglada, *Int. Rev. Phys. Chem.*, 2011, **30**, 335–369.
33 S. Aloisio, J. S. Francisco and R. R. Friedl, *J. Phys. Chem. A*, 2000, **104**, 6597–6601.
34 C. P. Ennis, J. R. Lane, H. G. Kjaergaard and A. J. McKinley, *J. Am. Chem. Soc.*, 2009, **131**, 1358–1359.
35 D. Stone and D. M. Rowley, *Phys. Chem. Chem. Phys.*, 2005, **7**, 2156–2163.
36 D. Stone, L. K. Whalley and D. E. Heard, *Chem. Soc. Rev.*, 2012, **41**, 6348–6404.
37 X. Chen, C. Tao, L. Zhong, Y. Gao, W. Yao, S. Li and S. Chem, *Phys. Lett.*, 2014, **608**, 272–276.
38 L. P. Viegas and A. J. C. Varandas, *Chem. Phys.*, 2012, **399**, 17–22.
39 L. P. Viegas and A. J. C. Varandas, *Eur. Phys. J. D*, 2016, **70**, 48.
40 N. Goldman, R. S. Fellers, C. Leforestier and R. J. Saykally, *J. Phys. Chem. A*, 2001, **105**, 515–519.
41 M. E. Dunn, E. K. Pokon and G. C. Shields, *J. Am. Chem. Soc.*, 2004, **126**, 2647–2653l.
42 M. J. Frisch, G. Trucks and J. A. Pople, *et al.*, *Gaussian 09, Revision A.01*, Gaussian Inc, Pittsburgh, PA, 2009.
43 M. Walker, A. J. A. Harvey, A. Sen and C. E. H. Dessent, *J. Phys. Chem. A*, 2013, **117**, 12590–12600.
44 Y. Zhao and D. G. Truhlar, *Theor. Chem. Acc.*, 2008, **120**, 215–241.
45 N. Bork, L. Du, H. Reiman, T. Kurten and H. G. Kjaergaard, *J. Chem. Phys. A*, 2014, **118**, 5316–5322.
46 F. Y. Liu, X. F. Tan, Z. W. Long, B. Long and W. J. Zhang, *RSC Adv.*, 2015, **5**, 32941–32949.
47 C. Gonzalez and H. B. Schlegel, *J. Chem. Phys.*, 1989, **90**, 2154–2161.
48 M. Page and J. W. McIver Jr, *J. Chem. Phys.*, 1988, **88**, 922–935.
49 K. Fukui, *Acc. Chem. Res.*, 1981, **14**, 363–368.
50 Y. S. Lee, S. A. Kucharski and R. J. Bartlett, *J. Chem. Phys.*, 1984, **81**, 5906–5912.
51 A. J. C. Varandas and F. N. N. Pansini, *J. Chem. Phys.*, 2014, **141**, 224113.
52 B. C. Garrett and D. G. Truhlar, *J. Chem. Phys.*, 1979, **70**, 1593–1598.
53 B. C. Garrett and D. G. Truhlar, *J. Am. Chem. Soc.*, 1979, **101**, 4534–4548.
54 B. C. Garrett, D. G. Truhlar, R. S. Grev and A. W. Magnuson, *J. Phys. Chem.*, 1980, **84**, 1730–1748.
55 Y. P. Liu, G. C. Lynch, T. N. Truong, D. H. Lu, D. G. Truhlar and B. C. Garrett, *J. Am. Chem. Soc.*, 1993, **115**, 2408–2415.
56 D. Lu, T. N. Truong, V. S. Melissas, G. C. Lynch, Y. P. Liu, B. C. Garrett, R. Steckler, A. D. Isaacson, S. N. Rai, G. C. Hancock, J. G. Lauderdale, T. Joseph and D. G. Truhlar, *Comput. Phys. Commun.*, 1992, **71**, 235–262.
57 S. W. Zhang and N. T. Truong, *VKLab version 1.0*, University of Utah, Salt Lake City, 2001.
58 D. L. Singleton and R. J. Cvetanovic, *J. Am. Chem. Soc.*, 1976, **98**, 6812–6819.
59 From the NIST chemistry webbook, http://webbook.nist.gov/chemistry.
60 T. L. Zhang, W. L. Wang, P. Zhang, J. Lü and Y. Zhang, *Phys. Chem. Chem. Phys.*, 2011, **13**, 20794–20805.
61 J. L. Bao, P. Seal and D. G. Truhlar, *Phys. Chem. Chem. Phys.*, 2015, **17**, 15928–15935.
62 X. Chen, Y. F. Zhao, L. S. Wang and J. Li, *Comput. Theor. Chem.*, 2017, **1107**, 57–65.
63 Y. Zhao, X. Chen and J. Li, *Nano Res.*, 2017, **10**, 3407–3420.
64 T. L. Zhang, X. G. Lan, Z. Y. Qiao, R. Wang, X. H. Yu, Q. Xu, Z. Y. Wang, L. X. Jin and Z. Q. Wang, *Phys. Chem. Chem. Phys.*, 2018, **20**, 8152–8165.
65 K. S. Alongi, T. S. Dibble, G. C. Shields and K. N. Kirschner, *J. Phys. Chem. A*, 2006, **110**, 3686–3691.
66 B. Long, X. Tan, Z. Long, Y. Wang, D. Ren and W. Zhang, *J. Phys. Chem. A*, 2011, **115**, 6559–6567.
67 J. Gonzalez, M. Torrent-Sucarrat and J. M. Anglada, *Phys. Chem. Chem. Phys.*, 2010, **12**, 2116–2125.

